

1 **Robust and irreversible impacts of an AMOC collapse**
2 **on tropical monsoon systems: a multi-model**
3 **comparison**

4 **M. Ben-Yami^{1,2}, P. Good³, L. C. Jackson³, M. Crucifix⁴, A. Hu⁵, O. Saenko**
5 **⁶, D. Swingedouw⁷ and N. Boers^{1,2,8}**

6 ¹Earth System Modelling, School of Engineering and Design, Technical University of Munich, Munich,
7 Germany

8 ²Potsdam Institute for Climate Impact Research, Potsdam, Germany

9 ³Met Office, Exeter, UK

10 ⁴Earth and Life Institute, UCLouvain, Place Louis Pasteur 3, Louvain-La-Neuve, 1348, Belgium

11 ⁵Climate and Global Dynamics Lab, National Center for Atmospheric Research, Boulder, CO 80307, USA

12 ⁶SEOS, University of Victoria, BC, Canada

13 ⁷Environnements et Paléoenvironnements Océaniques et Continentaux (EPOC)— Université de
14 Bordeaux, Pessac, France

15 ⁸Department of Mathematics and Global Systems Institute, University of Exeter, Exeter, UK

16 **Key Points:**

- 17 • A collapse of the AMOC would cause a major rearrangement of all tropical mon-
18 soon systems
- 19 • Four state-of-the-art climate models show remarkable agreement on the effects of
20 an AMOC collapse
- 21 • These impacts are practically irreversible

Corresponding author: M. Ben-Yami, maya.ben-yami@tum.de

Abstract

A collapse of the Atlantic Meridional Overturning Circulation (AMOC) would have substantial impacts on global precipitation patterns, especially in the vulnerable tropical monsoon regions. We assess these impacts using four state-of-the-art climate models with bistable AMOC. Spatial and seasonal patterns of precipitation change are remarkably consistent across models. We focus on the South American Monsoon (SAM), the West African Monsoon (WAM), the Indian Summer Monsoon (ISM) and the East Asian Summer Monsoon (EASM). Models consistently suggest substantial disruptions for WAM, ISM and EASM with shorter wet and longer dry seasons (-29.07%, -18.76% and -3.78% ensemble mean annual rainfall change, respectively). Models also agree on changes for the SAM, suggesting rainfall increases overall, in contrast to previous studies. These are more pronounced in the southern Amazon (+43.79%), accompanied by decreasing dry-season length. Consistently across models, our results suggest major rearranging of all tropical monsoon systems in response to an AMOC collapse.

Plain Language Summary

The Atlantic Meridional Overturning Circulation (AMOC) is a key element of the Earth's climate system, transporting large amounts of heat and salt northward in the upper layers of the Atlantic ocean. Although its likelihood remains highly uncertain, a collapse of the AMOC in response to anthropogenic climate change would have catastrophic ecological and societal consequences. This is especially true in the vulnerable monsoon regions of the tropics. Yet, the precise effects of an AMOC collapse on the tropical monsoon systems remain unclear. We take advantage of a climate model intercomparison project, and provide a detailed and systematic analysis of the irreversible seasonal impacts of an AMOC collapse on the major tropical monsoon systems. We find remarkable, previously unseen, agreement between four independent state-of-the-art climate models. Consistently across models, our results suggest major rearranging of all tropical monsoon systems in response to an AMOC collapse.

1 Introduction

The Atlantic Meridional Overturning Circulation (AMOC) is a key element of the Earth's climate system, transporting large amounts of heat and salt northward in the upper layers of the Atlantic ocean. Paleoclimate proxy evidence as well as theoretical considerations suggest that the AMOC is bistable, with a second, substantially weaker circulation mode in addition to the present strong mode (Henry et al., 2016; Stommel, 1961; Rahmstorf, 2002). The question whether the AMOC is bistable in comprehensive climate models has been intensely debated in recent years and a rising number of such models exhibit a bistable AMOC (Y. Liu et al., 2014; W. Liu et al., 2017; Jackson & Wood, 2018; Romanou et al., 2023). Concerns have been raised that the AMOC might collapse to its weak state in response to enhanced freshwater inflow into the North Atlantic due anthropogenic warming and resulting Greenland ice sheet melting (W. Liu et al., 2017), although the 6th assessment report (AR6) of the International Panel on Climate Change (IPCC) concludes that such a collapse has moderate likelihood to happen before 2100 (Arias et al., 2021). Studying a potential AMOC collapse is however of great interest given the severe global impacts it would have. There are several lines of proxy-based evidence suggesting that the AMOC has indeed weakened in the last decades to centuries (Caesar et al., 2021) and comprehensive models predict that it will weaken further under anthropogenic global warming (Lee et al., 2021). In addition, evidence that the recent AMOC weakening might be associated with a decrease of stability of the current circulation mode has been identified in sea-surface temperature (SST) and salinity based fingerprints of the AMOC strength (Boers, 2021).

71 If the AMOC were to collapse, the reduced northward heat transport would cause
72 a relative cooling of the northern hemisphere, and the change in inter-hemispheric en-
73 ergy transport would lead to a shift of the thermal equator and hence a southward shift
74 of the inter-tropical convergence zone (ITCZ) (Jackson et al., 2015). The subsequent global-
75 scale reorganization of the atmospheric circulation would have far-reaching effects in the
76 Pacific as well as in the Atlantic (Orihuela-Pinto et al., 2022). As the ITCZ is the main
77 source of tropical rainfall, an AMOC collapse and associated southward ITCZ shift would
78 likely have substantial consequences for the tropical monsoon systems. Given their so-
79 cioeconomic and ecological importance, a detailed analysis of the impacts of an AMOC
80 collapse on these monsoon systems is needed. Over half of the world's population live
81 in climates dominated by tropical monsoons (Moon & Ha, 2020; Wang et al., 2021). Most
82 of these are in developing countries, where land use is dominated by agriculture, so de-
83 pends heavily on the rain the monsoons bring. These regions are thus vulnerable to any
84 changes in the characteristics of the monsoon rains, whether they are changes in the tim-
85 ing or the amount of rainfall (WRCP, n.d.). This makes tropical monsoon regions a high
86 priority regarding possible impacts of anthropogenic global warming (Wang et al., 2021).

87 There exist multiple lines of proxy evidence to assess the impacts of an AMOC col-
88 lapse on the tropical monsoon systems during past climate conditions (Sun et al., 2012;
89 Sandeep et al., 2020; Häggi et al., 2017; Mosblech et al., 2012; Wassenburg et al., 2021;
90 Marzin et al., 2013). To study the effects in more detail and for present-day climate con-
91 ditions, so-called hosing experiments in general circulation models (GCMs) are used, in
92 which freshwater is added to a region of the north Atlantic for a long period of time, forc-
93 ing the AMOC to weaken and potentially collapse to a weaker state. Some studies have
94 also focused on individual monsoon systems such as the South American Monsoon (SAM)
95 (Good et al., 2021; Parsons et al., 2014), the West African Monsoon (WAM) (Chang et
96 al., 2008), the Indian Summer Monsoon (ISM) (Sandeep et al., 2020; Marzin et al., 2013)
97 and the East Asian Summer Monsoon (EASM) (Yu et al., 2009). Most studies find an
98 overall decrease in annual mean precipitation of the different monsoon systems. For trop-
99 ical South America, however, older simulations suggesting increased annual rainfall sums
100 (Stouffer et al., 2006) are in contrast with more recent modelling studies suggesting de-
101 creases (Jackson et al., 2015). In addition, both Parsons et al. (2014) and Good et al.
102 (2021) note that it is important to analyse the atmospheric response throughout the sea-
103 sonal cycle. Specifically, Parsons et al. (2014) find that a wetter dry season after an AMOC
104 collapse increased the overall Amazon vegetation productivity. The overall sign of the
105 precipitation change over tropical South America in response to an AMOC collapse re-
106 mains debated. This debate is complicated by the fact that there has been no cross-model
107 AMOC hosing comparison since (Stouffer et al., 2006), and in general it is difficult to
108 compare the impacts in experiments with different hosing scenarios.

109 The bi-stability of the AMOC has long been supported by theory, simple and intermediate-
110 complexity models (Stommel, 1961; Rahmstorf et al., 2005), as well as the paleoclimate
111 data record (Rahmstorf, 2002; Henry et al., 2016). Nevertheless, many GCMs do not ex-
112 hibit the hysteresis associated with bi-stability (Y. Liu et al., 2014; Drijfhout et al., 2011),
113 although more recent studies do find a persistent weak state (Jackson & Wood, 2018;
114 Romanou et al., 2023). The North Atlantic Hosing Model Intercomparison Project (NA-
115 HosMIP) compares eight different models from the sixth phase of the Climate Model In-
116 tercomparison Project (CMIP6), aiming to investigate AMOC response and associated
117 hysteresis (Jackson et al., 2022). Four out of the eight studied models exhibit a bistable
118 AMOC, and this allows for a unique opportunity to investigate the effects of an AMOC
119 collapse across models. Not only do all four models use the same hosing scenario, but
120 the bistability of their AMOC allows us to investigate the permanent and practically ir-
121 reversible impacts of the stable weak AMOC state that occurs after the hosing has been
122 stopped. This is in contrast to most AMOC hosing studies, in which the hosing is con-
123 tinuously applied during the study period.

124 The different models of NAHosMIP exhibit a range of different patterns and bi-
 125 ases, and thus comparing the effect of an AMOC collapse across models allows us to make
 126 robust statements on its effect on tropical precipitation. In this study we use results from
 127 the four models in NAHosMIP that remain in the weak state after the hosing is stopped:
 128 HadGEM3-GC3-1MM, CanESM5, CESM2 and IPSL-CM6A-LR (hereafter abbreviated
 129 as HadGEM, CanESM, CESM and IPSL). We compare spatial precipitation fields from
 130 the the control runs of these models (piControl) to scenarios in which a constant 0.3 Sv
 131 of hosing is applied over the North Atlantic for 50 years (100 years for the IPSL model),
 132 thus weakening the AMOC. After the hosing is stopped the AMOC remains in the weak
 133 state (see Methods for more details).

134 2 Results

135 2.1 Global change in precipitation

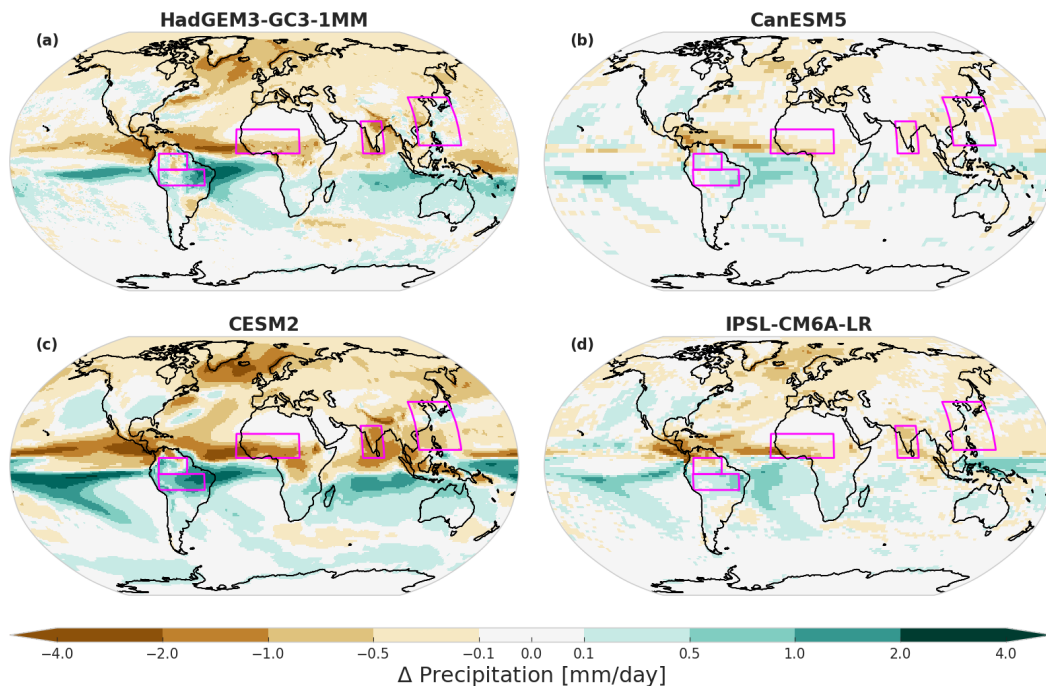


Figure 1. Modelled impacts of an AMOC collapse on global precipitation. Average precipitation shifts (weak AMOC run minus piControl run) for a. HadGEM3, b. CanESM, c. CESM, and d. IPSL. Note the southward ITCZ shift and the general pattern of Northern-Hemisphere drying and Southern-Hemisphere wetting in response to an AMOC collapse, shared by all models. The magenta boxes show the monsoon regions investigated in this work: the two parts of the SAM as well as the WAM, ISM, and EASM (see Methods and Table S1).

136 The model control runs have biases when compared to observations (see Figure S1).
 137 To understand the effect of an AMOC collapse on global precipitation, it is therefore more
 138 informative to analyse the differences between the post- and pre-hosing model runs than
 139 between the post-hosing runs and observations. In the following we will in general refer
 140 to the post-hosing collapsed state as the weak AMOC. The resulting pattern of global
 141 precipitation post shifts in response to an AMOC collapse is then remarkably similar in all
 142 four models (Figures 1(a)-(d) and S2): (i) a southward shift of the ITCZ and overall in-
 143 creased (decreased) precipitation over the southern (northern) hemisphere; (ii) a gen-

144 eral reduction of precipitation of the higher latitudes; (iii) reduced precipitation in all
 145 monsoon regions except the SAM; and (iv) increased precipitation over most of the Ama-
 146 zon, especially in the east.

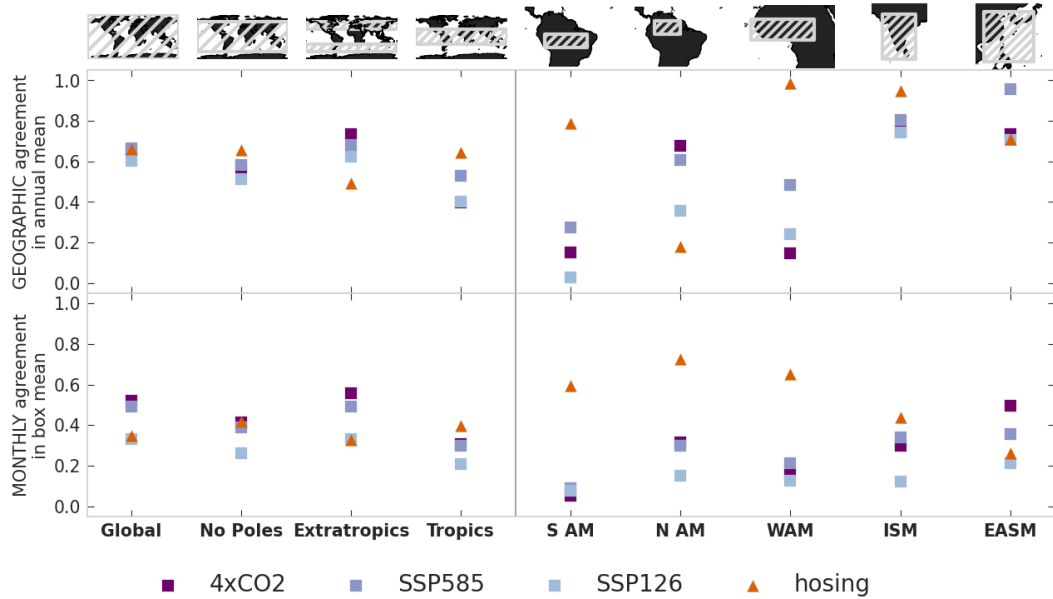


Figure 2. Model agreement in the NAHosMIP experiments compared to the agreement in CMIP6 warming experiments. (a) The fraction of gridcells in a given geographic region that agree on the sign of change in the annual mean rainfall. (b) The fraction of months in a year that agree on the sign of change in the mean monthly rainfall in the given box. The square markers show the agreement for the 4xCO₂ (purple), SSP585 (lilac) and SSP126 (light blue) experiments. The triangular orange marker shows the agreement of the hosing experiments. The regions of analysis are defined in Tables S1 and S2, and are shown as grey dashed boxes on the maps in the top row. A horizontal grey line separates the values for the global boxes from the regional monsoon boxes. The exact values are given in Tables S2 and S3.

147 The four models show a remarkable agreement on the sign of precipitation changes
 148 in the tropics (20°S-20°N) in response to an AMOC collapse. The fraction of land in which
 149 the sign of change is consistent in the four models is 0.64 in the tropics, and is as large
 150 as 0.99 in some of the individual monsoon regions (see Table S2 and Figure 2). The agree-
 151 ment in the seasonal cycle change is also especially high in the Atlantic monsoon regions
 152 (Table S3). Notably, in the tropics the agreement between these four models on the im-
 153 pacts of an AMOC collapse are consistently higher than the agreement found in differ-
 154 ent CMIP6 warming experiments (Figure 2). As CMIP6 models are known to have in-
 155 consistent precipitation predictions in the tropics (Lee et al., 2021; Moon & Ha, 2020;
 156 Wang et al., 2021), the higher agreement found in the hosing experiments is even more
 157 remarkable.

158 Whilst the overall pattern of change in the four models subsequent to an AMOC
 159 collapse is in agreement, the magnitude of the precipitation change varies. CanESM and
 160 IPSL have a comparably small change in precipitation following an AMOC collapse, of
 161 the order of 0.5 mm/day in the monsoon regions (Figure 1). The model with the largest
 162 precipitation change is CESM, with a precipitation change over the SAM, ISM and WAM
 163 in CESM of the order of 2-3 mm/day, with a slightly smaller change in the EASM. HadGEM

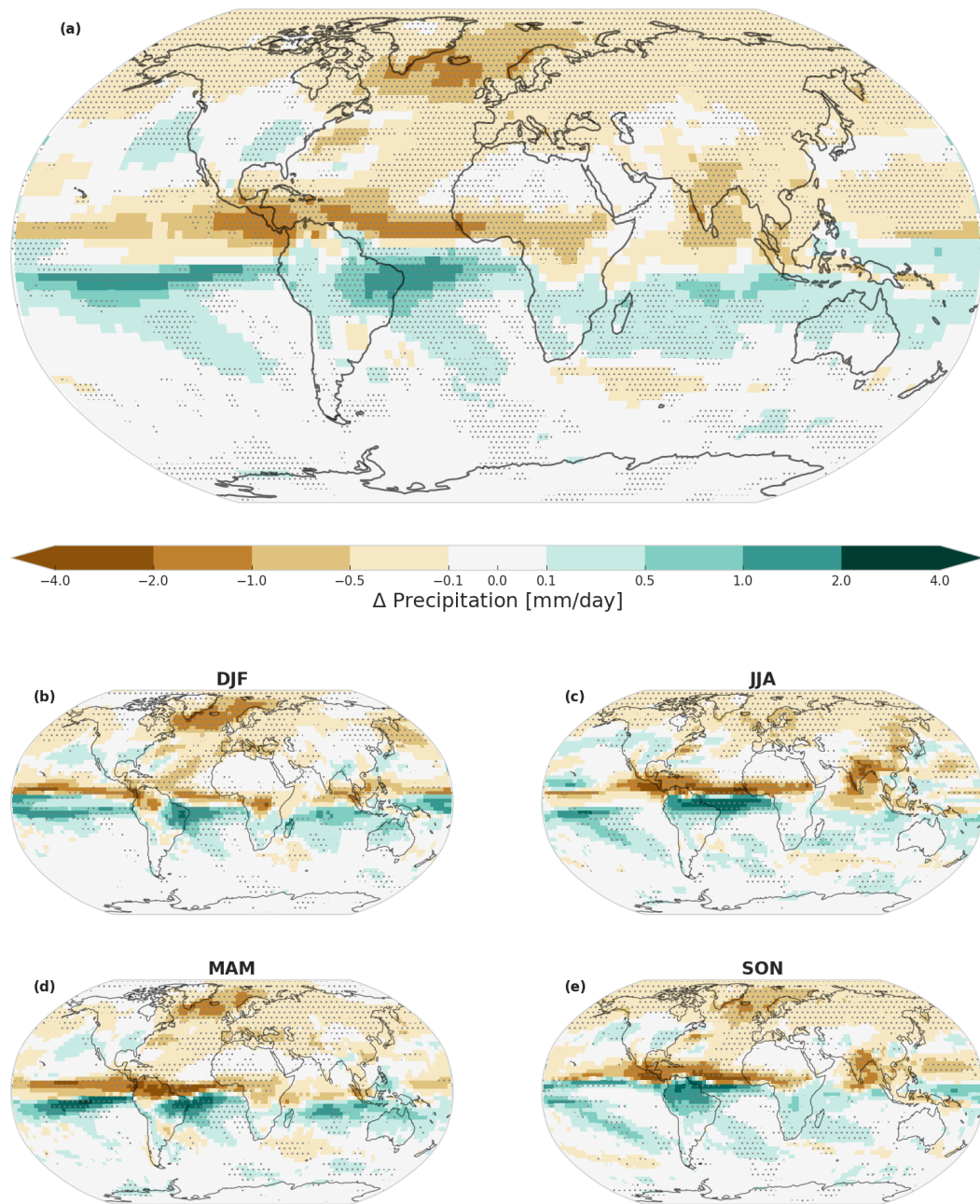


Figure 3. Average precipitation anomaly (weak AMOC run minus piControl run) for the ensemble mean of the four models. Figure (a) shows the annual mean, whilst Figures (b)-(e) show the season anomalies in DJF, JJA, MAM and SON, respectively. The stippling in each Figure indicates regions in which all four model anomalies agree in sign for that mean.

164 is midway between the two extremes with changes on the order of 1 mm/day. HadGEM
 165 also has a more complex precipitation change pattern for the SAM, with less rainfall over
 166 about half of the northern Amazon region and more rainfall over the rest of the region.

167 Even in light of the differences in magnitude, the agreement between the models
 168 is remarkable, given that previous generations of models have shown considerably stronger
 169 differences and inconsistencies (for example, Jackson et al. (2015) showed a drying over
 170 almost all of the Amazon, in contrast to the multi-model comparison in (Stouffer et al.,
 171 2006)). This similarity in our models justifies a calculation of the ensemble mean pre-
 172 cipitation anomaly (Figure 3). The ensemble mean shows the same pattern as described
 173 above, with a drying of all monsoon regions except the SAM. The ensemble mean per-
 174 centage changes in rainfall in the monsoon regions are (Figure S2): +5.2% in the North-
 175 ern Amazon, +43.79% in the Southern Amazon, -29.07% in the WAM, -18.76% in the
 176 ISM and -3.78% in the EASM.

177 To understand the different magnitudes of model responses to an AMOC collapse
 178 we analyse the seasonal cycle of the Atlantic ITCZ following (Good et al., 2021) (see Meth-
 179 ods). A smaller shift of the Atlantic ITCZ after an AMOC collapse should result in a
 180 smaller precipitation anomaly, and this is reflected in the respective Atlantic ITCZ shifts
 181 of the models (Figure S3 (a)-(d)). IPSL and CanESM have only a small ($\leq 1^\circ$) latitu-
 182 dinal shift in the Atlantic ITCZ between the control and weak AMOC, whilst the shift
 183 in HadGEM and CESM is a few times larger. The latter two also have a seasonal At-
 184 lantic ITCZ cycle which is closer to the observations (see Methods for details). The or-
 185 dering of magnitudes is also mirrored in the amount the model AMOC weakens from the
 186 piControl to the weak state in the respective models (Figure S4).

187 2.2 Changes in the seasonal cycle

188 Whilst the pattern of annual mean rainfall anomaly is informative for understand-
 189 ing the global effect of an AMOC collapse, the effect on the major tropical monsoon sys-
 190 tems is by definition highly seasonally dependent. We investigate the seasonal change
 191 in rainfall in two ways. First, calculating the average seasonal cycle in the whole of a given
 192 monsoon region, and second, calculating the geographic pattern of change in dry and wet
 193 seasons in these regions.

194 All piControl model runs match the overall pattern of the observed seasonal rain-
 195 fall, but there are considerable biases in some cases (Figure 4). Their strengths depend
 196 on the region and model, with no model standing out as the best one in matching the
 197 observations across regions. For example, the best match between observations and con-
 198 trol runs for the WAM and ISM is in CESM, but CanESM reproduces the southern Ama-
 199 zon rainfall better. CanESM, on the other hand, has the largest biases of any model in
 200 the northern Amazon and the ISM, with a difference of over 6 mm/day in the ISM wet
 201 season.

202 As discussed above, the sign of this monthly precipitation change is overall in agree-
 203 ment between models (Figures 2b and S5b and Table S3). In general there is high agree-
 204 ment in the hosing experiments for the SAM and WAM and slightly less for the ISM and
 205 EASM, which is likely due to the former being directly impacted by the southward shift
 206 of the Atlantic ITCZ.

207 The pattern of seasonal cycle change present in these models is: (i) The southern
 208 Amazon gains a small amount of precipitation in all months, with the exception of CanESM
 209 showing a small precipitation decrease in the January-to-March part of the wet season
 210 (Figure 4a). The overall gains are in line with a southward shift of the Atlantic ITCZ,
 211 since this box extends from 5° S down to 15° S, that is, on the edge of the Atlantic ITCZ
 212 extent. A southward shift of the Atlantic ITCZ therefore brings more of the austral sum-
 213 mer precipitation into this area; (ii) The northern Amazon has the most complex pat-

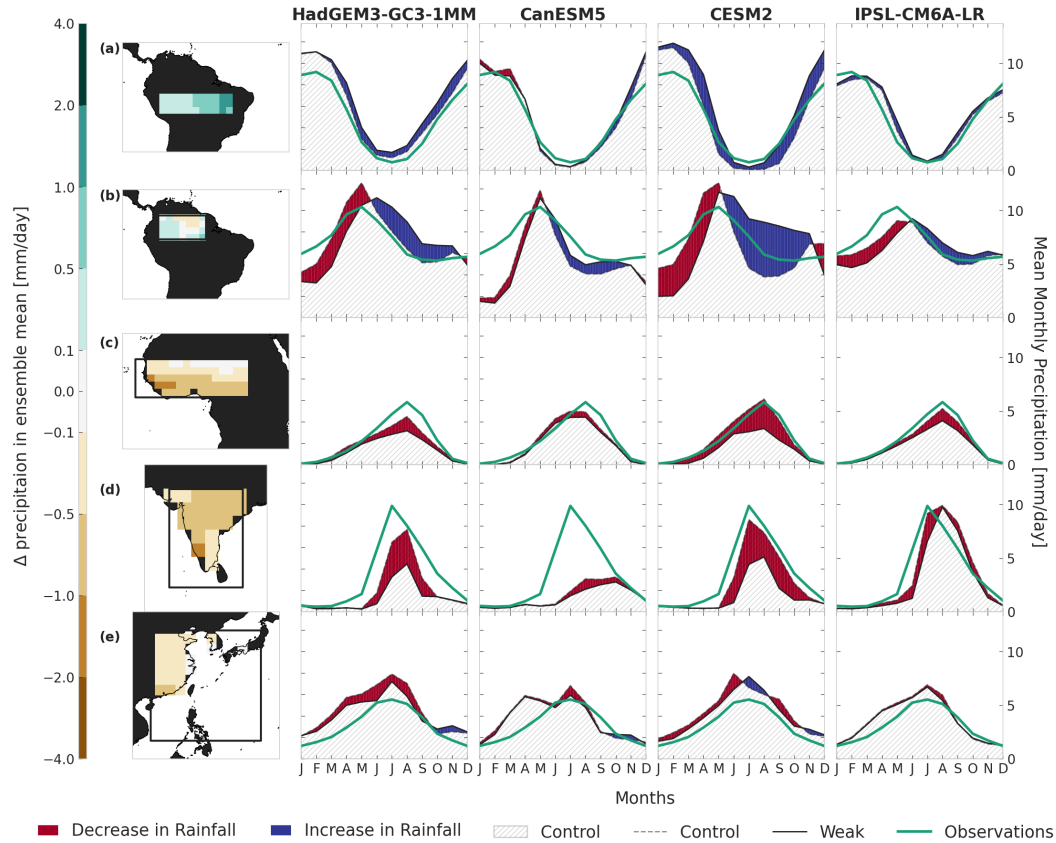


Figure 4. Changes in the seasonal cycle due to an AMOC collapse in two parts of the SAM (a,b), as well as in the WAM (c), ISM (d), and EASM (e). The first column shows the ensemble mean average yearly precipitation change in the given region (i.e., average over all four models). Taking this ensemble mean is justified by the high model agreement as identified above. The remaining columns show the change in precipitation from the average seasonal cycle in the pi-Control (dot-dashed line) to the weak AMOC run (solid line) for the four different models. The area under the graph is shaded in red where the rainfall decreases and in blue where it increases in response to an AMOC collapse. The area common to both is marked by black hatches. The observed seasonal cycle in shown as the turquoise line. Coordinates for the monsoon boxes can be found in Table S1.

214 tern, with reduced rainfall in the piControl wet season and increased rainfall in the pi-
 215 Control dry season (Figure 4b). This is due to a combined shift in time of the wet sea-
 216 son to later in the year and a reduction in the overall rainfall. It should be noted that
 217 this region also has a complex spatial pattern of changing rainfall in addition to the sea-
 218 sonal pattern (see Figures 1, 3 and 5); (iii) The WAM has a clear pattern (Figure 4c),
 219 showing decrease in rainfall during the wet season in all models. In CESM this is a 50%
 220 rainfall decrease, and in the other models closer to 5-10%. Since the WAM is at the north-
 221 ern edge of the Atlantic ITCZ range, such a drying is to be expected from a southward
 222 shift of the ITCZ; (iv) The ISM has a similar pattern to the WAM, with a substantial
 223 loss of rainfall during the wet season (Figure 4d); and (v) The EASM shows a general
 224 drying which is relatively small in all models. All models also show a small increase in
 225 dry-season rainfall, but both these changes are too small to change the amplitude, tim-

226 ing or structure of the overall seasonal cycle. CESM also shows a shift of the peak wet
 227 season rainfall from June to August (Figure 4e).

228 The magnitudes of all these changes in the different models are in line with the shift
 229 in the Atlantic ITCZ - the larger the shift, the larger the precipitation change, independ-
 230 ently of the piControl model bias.

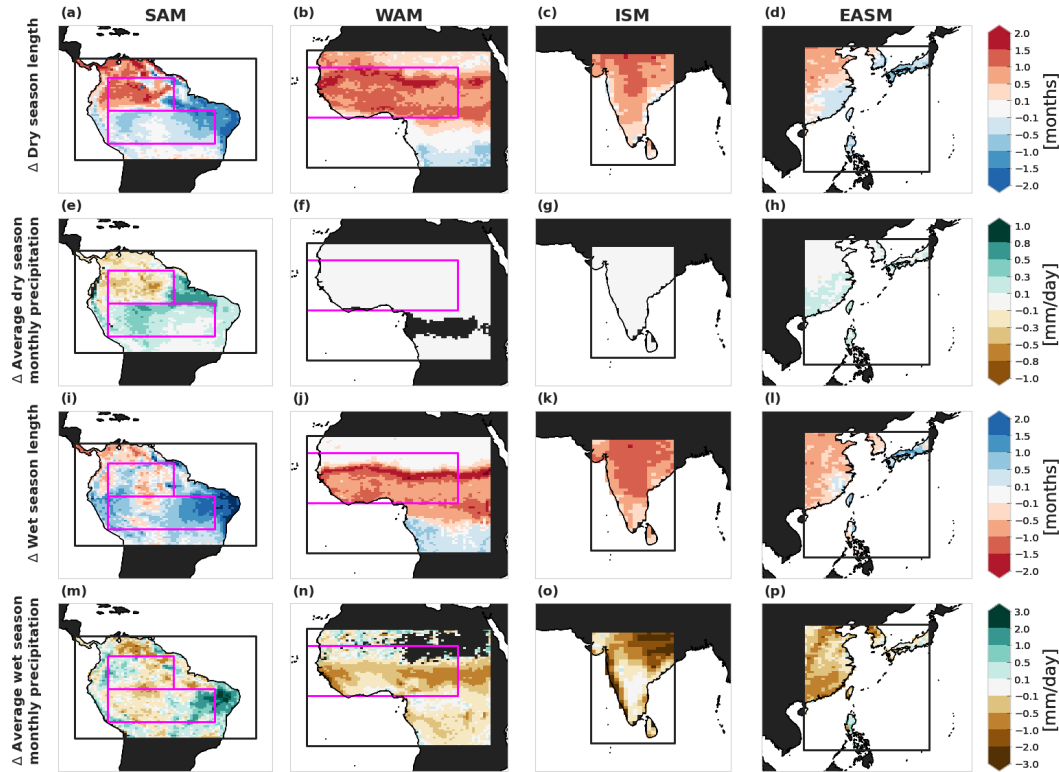


Figure 5. Changes in dry and wet season length and average monthly precipitation in HadGEM3-GC3-1MM, defined as the weak AMOC run value minus the piControl value. The four rows show the change in dry season length (a-d), average dry season monthly precipitation (e-h), wet season length (i-l) and average wet season monthly precipitation (m-p), respectively. Each column shows a different monsoon region, with the region used for defining the dry/wet season shown as a black box. See methods for further details. The magenta boxes show the regions used in Figure 4 if they are different from the black boxes. Note the scales for the change in dry and wet season lengths are inverted to match red/blue to less/more rain respectively. Some areas within the monsoon regions are black if neither model run has a dry/wet season in that area, according to our definition (see Methods). Coordinates of the boxes use to define the dry/wet season can be found in Table S4.

231 In the first column of Figure 4 and in Figure 1 it can be seen that while in general
 232 the sign of change is the same for the average as within the region, there is some spa-
 233 tial variation in the magnitude of the rainfall change. This spatial variation can be in-
 234 vestigated through the change in the characteristics of the dry and wet seasons in the
 235 four regions. We define the dry (wet) season as the months with rainfall below (above)
 236 the 40th (60th) percentile of the whole region (see Methods for full details). Changes in
 237 dry- and wet-season rainfall and length caused by an AMOC collapse are shown only for
 238 HadGEM for the sake of clarity, as it has the most realistic Atlantic ITCZ (see Figure

239 S3) and highest spatial resolution (Figure 5). Note that the changes in precipitation in
 240 HadGEM are highly correlated with the changes in the other models in the monsoon re-
 241 gions (see Methods and Fig S6 and S7). The results agree with our previous findings:
 242 a general drying of the WAM, ISM and EASM through a longer dry season and a shorter
 243 wet season, and a more complex pattern for the SAM. In particular,

244 (i) the northern Amazon has a similar or longer dry season and a shorter wet sea-
 245 son in most regions. The average dry season month also shows a reduction in precipi-
 246 tation. The wet season months are wetter in the western part, and drier in the eastern
 247 part, matching the pattern seen in the yearly mean (Figure 1). Yet, the rainfall reduc-
 248 tion over the eastern part of the northern Amazon is only shown by HadGEM (Figure S7);

249 (ii) the southern Amazon shows a shorter and wetter dry season, but has a mixed
 250 pattern for the wet season. The western part of the southern Amazon generally has a
 251 drier and shorter wet season. The overall increase in wet season rainfall is related to the
 252 longer and much wetter wet season of the eastern edge of the southern Amazon. All pi-
 253 Control runs show a strong wet bias compared to observations in this southeastern Ama-
 254 zon region (Figure S1), so the change in rainfall might not be accurate;

255 (iii) in Africa, the WAM region is where the largest changes occur, with a longer
 256 dry season and a shorter wet season, especially at the southern edge of the Sahel. There
 257 is negligible change in the dry season monthly precipitation (which was already close to
 258 zero), but there is a reduction in the wet season precipitation. The only outlier is the
 259 Congo region, which benefits from a shorter dry season and a longer (but drier) wet
 260 season due to the southward shift of the Atlantic ITCZ;

261 (iv) for the ISM, the drying is more predominant in the wet season. While the dry
 262 season is longer by up to one month inland, the wet season is shorter by at least a month
 263 almost everywhere and has significantly drier months in the north-east;

264 (v) the EASM has a mixed change in the dry season: the northern part has a longer
 265 and the southern a shorter dry season, with little change in the average precipitation.
 266 The overall drying is more drastic in the wet season, similarly to the ISM, with an over-
 267 all shorter wet season and drier months.

268 **3 Discussion and Conclusions**

269 The four monsoon systems investigated in this work are vital parts of the global
 270 climate. Nearly three-quarters of the world's population is affected by monsoons, mak-
 271 ing them a high priority regarding possible impacts of anthropogenic global warming.
 272 This work is the first one to compare the effect of an AMOC collapse on monsoon sys-
 273 tems in multiple CMIP6 GCM experiments which apply the same hosing scenario.

274 While the four models used in this study have different Atlantic ITCZ biases (Fig-
 275 ure S3), their agreement on the pattern of the precipitation response to an AMOC col-
 276 lapse (Figures 2, S5 and S6 and Tables S2 and S3) is a strong case for the robustness of
 277 that pattern (Figures 1 and 3).

278 The overall response structures are remarkably consistent across models, both ge-
 279 ographically and seasonally (Figure S5). The WAM, ISM and EASM show an overall dry-
 280 ing with a shorter wet season and longer dry season in response to an AMOC collapse.
 281 The SAM shows a more spatially dependant pattern, with an overall annual increase in
 282 rainfall, a higher increase of annual precipitation and shorter dry season in the south and
 283 less pronounced change in the north.

284 The year-long reduction in precipitation associated with WAM, ISM and EASM
 285 would likely have severe ecological and socio-economic impacts. The effect of an AMOC
 286 collapse on the SAM and, hence, on the Amazon rainforest, is more uncertain. (Parsons

et al., 2014) showed that even with an overall decrease in yearly rainfall sums over the region, a shorter dry season leads to increased productivity in the Amazon rainforest. However, the effect on the SAM dry season shown in this work is complex: in the northern Amazon, there is a shift of the seasonal cycle to later in the year in all models, and also an increase in dry season length. To understand the effect this would have on the rainforest requires additional modelling considering the vegetation response. On the other hand, the effect on the southern Amazon is different: more overall rainfall and a shortened and wetter dry season. This southern Amazon region is also the one shown to be losing resilience faster in the past decades (Boulton et al., 2022) and therefore may be more susceptible to changes in rainfall. This relative complexity in Amazon rainfall response may be the reason for the contrasting results of past models (Stouffer et al., 2006; Jackson et al., 2015) with regards to the effect of an AMOC collapse on the Amazon. The agreement of four different GCM experiments allows us to conclude that the overall effect of an AMOC collapse on the Amazon could counteract precipitation reductions projected for future global warming scenarios (see Arias et al. (2021)).

This work presents the effects of an AMOC collapse in tropical monsoon systems, inferred from simulations of the NAHosMIP project. Detailed analyses of many of the relevant physical processes at play in the models have already been presented in works on earlier hosing experiments, and have been identified in our results (Orihuela-Pinto et al., 2022; Good et al., 2021; Chang et al., 2008; Yu et al., 2009).

There is considerable uncertainty in the impact future global warming will have on monsoon rainfall (Arias et al., 2021; Wang et al., 2021; Moon & Ha, 2020). We show that our models agree much more for AMOC hosing experiments than they do for other CMIP6 warming experiments. Our work thus allows us to constrain projections in this high-uncertainty region.

The key property of the impacts discussed in this work is that they are practically irreversible. Whilst the direct impacts on monsoon rainfall from anthropogenic forcing could be reversed if the temperature is returned to pre-industrial levels, the collapse of the AMOC is permanent in the experiments considered in this study, something that was not certain in many previous hosing experiments. The impacts presented in this work could thus represent practically irreversible long-term changes that would persist even after a return to pre-industrial conditions.

Regardless of whether or not it is combined with increased temperatures, an AMOC collapse would result in a major rearranging of the global monsoon systems. This work shows that this rearrangement will have unfavorable effects on the WAM, ISM and EASM and a more uncertain effect on the SAM and the Amazon rainforest.

Methods

Model runs and processing of the outputs

We use the uniform hosing experiments from the North Atlantic Hosing Model Intercomparison study (NAHosMIP, Jackson et al. (2022)). These experiments start from the respective pre-industrial control (piControl) runs of CMIP6 models, and apply a 0.3Sv uniform hosing from 50°N to the Bering Strait. This hosing is applied for a given length of time and then stopped, after which the model continues to run. In the models we consider, the AMOC remains in the weak state after the hosing is turned off. For HadGEM, CanESM and CESM, we use the u03-r50 experiments, in which the hosing has been halted after 50 years. For IPSL, we use the u03-r100 experiments, in which the hosing has been halted after 100 years.

For consistent comparison we use 80 years from each of the different model runs. As the AMOC takes a few years to settle into a stable state after the hosing is turned

off, we take the last 80 years from HadGEM and CanESM, years 100-180 from CESM and years 60-140 from IPSL. For all models we use the first 80 years from the piControl.

For the comparison with the observational GPCP dataset the model outputs are regridded to a regular 2.5° grid. For calculation of the ensemble mean the model outputs are regridded to the coarsest-resolution model grid, that of the CanESM5 model. When correlating the HadGEM3-GM3-1MM output with the other three models, the HadGEM outputs are regridded to the respective model grid. All regridding is done using a first order conservative remapping.

4xCO₂ experiments are taken from the CMIP6 abrupt-4xCO₂ experiments, where an instantaneous quadrupling of the pre-industrial atmospheric CO₂ concentration is imposed and this concentration is kept constant. As the AMOC takes a few years to react to this we take years 60-140 from all models, using 80 years for consistent comparison with the NAHosMIP runs. We also use the CMIP6 historical runs, in which the anthropogenic forcings of 1850-2014 are applied to the climate, starting from some point in the piControl run. For all models, the r1i1p1f1 ensemble member is used, with the exception of HadGEM3, for which r1i1p1f3 is used. This is also the case for the piControl and 4xCO₂ runs.

For the scenario-mip CMIP6 runs ssp585 and ssp126 we use years 2080-2100 for consistency across models. The same ensemble members are used as above, except for CESM2 where we use r4i1p1f1 in ssp126 and r10i1p1f1 in ssp585.

Observational Datasets

For comparison with model results and calculation of the ITCZ latitude (which requires precipitation data over land and sea), we use the GPCP Precipitation data provided by NOAA/OAR/ESRL PSL, Boulder, Colorado, USA (Adler et al., 2018) available for 1979-2020. For all other precipitation analyses we use the GPCP Full Data Monthly Product Version 2020 at 0.25° from 1921 to 2019 (the first 20 years are not used due to the paucity of measurements in the regions of interest) (Schneider et al., 2020).

For the observed AMOC strength (Figure S4) the RAPID AMOC monitoring project data is used (Frajka-Williams et al., 2021).

ITCZ calculation

The ITCZ latitude is calculated following Good et al. (2021) to evaluate the model performance and effect of AMOC collapse.

The Atlantic ITCZ latitude is calculated in the area $35-15^\circ\text{W}$ $15^\circ\text{S}-15^\circ\text{N}$ as a precipitation-weighted mean, as follows:

$$\phi_{itcz} = \sum_i \frac{P_{35-15^\circ\text{W},\phi_i} \cdot \phi_i}{P_{35-15^\circ\text{W},15^\circ\text{S}-15^\circ\text{N}}} \quad (1)$$

Where $P_{35-15^\circ\text{W},\phi_i}$ is the zonally averaged precipitation at latitude ϕ_i , and $P_{35-15^\circ\text{W},15^\circ\text{S}-15^\circ\text{N}}$ is the precipitation averaged over the whole region. Each latitude is thus weighted by the precipitation at that latitude.

The same procedure is repeated in the Indian and Pacific oceans for the following areas: $55^\circ\text{E}-95^\circ\text{E}$, $15^\circ\text{S}-15^\circ\text{N}$ and $120^\circ\text{E}-95^\circ\text{W}$, $15^\circ\text{S}-15^\circ\text{N}$, respectively.

The ITCZ and AMOC strength in the different models

When compared to the observed seasonal cycle of the Atlantic ITCZ (hereafter simply ITCZ) the models can be divided into two groups (Figure S3 (a)-(d)): (i) The CanESM

and IPSL piControl runs have ITCZ latitudes going much further south (around 8°) in the December – March season (DJFM) than in observations. Their ITCZ varies more than 13° in latitude in a year, whilst the change in the average ITCZ seasonal cycle in the observation is 8.5° . It turns out that these two models only have a small ($\leq 1^\circ$) latitudinal shift in the ITCZ between the control and weak AMOC; (ii) HadGEM and CESM have a more realistic seasonal cycle of the ITCZ latitude, where the southward bias of the piControl is about 1° for all months. Compared to the Atlantic Ocean, the biases in simulated ITCZ latitudes in the piControl run relative to the observations are smaller in the Indian and Pacific Oceans (see Fig S8).

On the other hand, those models which have a more realistic latitudinal shift are also those which have a stronger piControl AMOC at 26.5N : In CanESM and IPSL the piControl AMOC has a strength of 11.27 Sv and 12.49 Sv respectively, and a post-hosing weak AMOC of 6.53 Sv and 5.20 Sv (Figure S4). HadGEM and CESM, on the other hand, have a much stronger piControl AMOC at 16.46 Sv and 17.39, respectively, and a post-hosing AMOC at 5.82 Sv and 8.70 Sv. The RAPID array observational measurements of the AMOC strength at 26.5N have a mean of 16.9 ± 4.6 Sv in 2004-2020 (Frajka-Williams et al., 2021), closer to HadGEM and CESM than to the other two models. Note, however, that these are historical observations and thus include the effect of anthropogenic forcings, and cannot be directly compared with the piControl simulations.

However although the collapsed AMOC has a similar strength in all four models, there are still major differences between the post-collapsed ITCZ cycles of the two groups of models. It is more likely that other properties of the IPSL and CanESM models cause both an extended ITCZ excursion to the south and a weaker piControl AMOC. In the CMIP6 Atmospheric Model Intercomparison Project (AMIP) experiments CanESM and IPSL have a seasonal ITCZ cycle much closer to the observations, without the southward excursion (Fig S9). As the AMIP models are forced with historical SSTs, the biases in the piControl runs of CanESM and IPSL are likely due to either biases in the modelled SST fields or in the SST-precipitation interactions in these models. Note, however, that the AMIP models include historical forcings which are absent in the piControl runs. Thus, for a reliable estimate of the magnitude (and not only the sign) of the precipitation change due to an AMOC collapse, further work should focus on the differences in the AMOC and SST biases of the different models.

Defining dry and wet seasons

The dry and wet seasons are defined using a non-parametric approach for consistency across monsoon regions. First, percentile boundaries are calculated for each region using all gridpoints and years. The dry or wet season months in a given year and grid-point are then all the months that have less or more rain than the chosen percentile boundary of the region. The 40th and 60th percentile are chosen for the dry and wet season, respectively. The dry season percentile is chosen such that for the SAM the dry season monthly rainfall limit is about 100 mm, which is the mean monthly evapotranspiration value of tropical forests (below this value evapotranspiration exceeds rainfall, see (Carvalho et al., 2021)).

The averaged dry (wet) season length is then the mean of dry (wet) season length over all years. The total dry (wet) season precipitation is, accordingly, the sum of rainfall in all months of the season, which is again averaged over all years to give the average total dry (wet) season precipitation. However, when comparing seasonal rainfall across runs with different season lengths, the total precipitation will be biased by the difference in season length. An average dry (wet) season monthly precipitation value is therefore defined by dividing the total dry (wet) season rainfall in a year by the length of the dry (wet) season in that year, and the average is calculated as

$$p_{i,\text{dry,avg}} = \frac{1}{T} \sum_{t=1}^T \frac{p_{i,t,\text{dry}}}{x_{i,t,\text{dry}}}, \quad (2)$$

426 where $p_{i,t,\text{dry}}$ and $x_{i,t,\text{dry}}$ are respectively the total dry season precipitation and dry
427 season length in grid-point i in year t , and the sum is over all years T .

428 When comparing these values between the piControl and weak AMOC model runs,
429 there are two ways to define the dry (wet) season for the weak AMOC run. The first is
430 to use the regions' percentile boundary values calculated for the piControl run, and ap-
431 ply them as the limit defining the weak AMOC seasons. The second is to independently
432 calculate new percentiles for the weak AMOC precipitation and use those as the defin-
433 ing limits. The first option reflects the experience of an abrupt change in the AMOC,
434 as it shows how the "known" seasons would change after a collapse. The second is more
435 applicable to an analysis of a long-term state, as it shows what the dry (wet) season would
436 look like in a world with a weak AMOC. As we are interested in the effect of an abrupt
437 collapse on ecosystems and societies which are in general adapted to a given pattern and
438 strength of seasonal rainfall, the value of interest will be the first one, which reflects how
439 the known seasons would change.

440 **Model bias**

441 Figure S1 shows the difference between the piControl run for the four models and
442 the global GPCP observations. The pattern in the yearly average precipitation bias is
443 as follows: (i) For the SAM all models except HadGEM show an $\sim 2\text{mm/day}$ dry bias,
444 whilst HadGEM shows a weak wet bias in the southern Amazon and a weak dry bias in
445 the northern Amazon; (ii) For the WAM there is a small dry bias in all four models; (iii)
446 For the ISM HadGEM and CanESM have a dry bias everywhere, whilst CESM and IPSL
447 have a dry bias in the north and a wet bias in the south; (iv) For the EASM all mod-
448 els except IPSL have a wet bias, whilst IPSL has a small dry bias. The piControl run
449 is the starting point with which we compare the collapsed AMOC state, so although the
450 observations are historical and thus include anthropogenic forcings not present in the pi-
451 Control runs, these comparisons are still informative.

452 **Agreement between HadGEM3-GC3-1MM and other models**

453 In Figure 5 the changes in dry and wet seasons are shown only for HadGEM. This
454 model was chosen due to its realistic Atlantic ITCZ and its higher spatial resolution. To
455 justify the use of HadGEM as representative of all models, Figure S7 shows the regions
456 in which all three other models or two of the other three models show the same sign of
457 precipitation anomaly as HadGEM, and Table S5 shows the correlation of the other mod-
458 els with HadGEM. These figures show the remarkable agreement between the models.
459 The only region in the monsoon areas of interest where HadGEM does not agree with
460 the other models is in the northeastern Amazon, where HadGEM shows a slight over-
461 all drying. However, it can be seen that the detailed seasonal response of precipitation
462 in that region is the same in all four models (Figure 4). The annual mean in this region
463 is the combined effect of a drying in January to June and increased rainfall in the rest
464 of the year. It is likely that the dry region in HadGEM has a different ratio between these
465 two effects than in the other models, but in practice has a similar response.

466 **4 Open Research**

467 The NAHosMIP model data is available at <https://doi.org/10.5281/zenodo.7324394>.
468 The pre-industrial control, 4xCO2 and AMIP experimental data is available via the Earth
469 System Grid Federation (ESGF) servers with information on obtaining data available

470 from <https://pcmdi.llnl.gov/CMIP6/Guide/dataUsers.html>. The GPCP and GPCC pre-
 471 cipitation datasets are available at <https://psl.noaa.gov/>. The RAPID observational data
 472 is available at <https://rapid.ac.uk/>. All code used to analyse the data and generate fig-
 473 ures will be uploaded at <https://github.com/mayaby>.

474 Acknowledgments

475 MBY and NB acknowledge funding by the European Union's Horizon 2020 research and
 476 innovation programme under the Marie Skłodowska-Curie grant agreement No.956170.
 477 NB acknowledges funding by the Volkswagen foundation. NB and LCJ acknowledge fund-
 478 ing by the TiPES project. This is TiPES contribution #X; the TiPES ('Tipping Points
 479 in the Earth System') project has received funding from the European Union's Horizon
 480 2020 research and innovation programme under grant agreement No. 820970. NB ac-
 481 knowledges further funding by the German Federal Ministry of Education and Research
 482 under grant No. 01LS2001A. OS thanks the CCCma team for support. LCJ was sup-
 483 ported by the Met Office Hadley Centre Climate Programme funded by BEIS and De-
 484 fra (grant GA01101).

485 References

- 486 Adler, R. F., Sapiano, M. R. P., Huffman, G. J., Wang, J.-J., Gu, G., Bolvin, D.,
 487 ... Shin, D.-B. (2018). The global precipitation climatology project (gpcp)
 488 monthly analysis (new version 2.3) and a review of 2017 global precipitation.
 489 *Atmosphere*, 9(4). Retrieved from [https://www.mdpi.com/2073-4433/9/4/](https://www.mdpi.com/2073-4433/9/4/138)
 490 138 doi: 10.3390/atmos9040138
- 491 Arias, P. A., Bellouin, N., Coppola, E., Jones, R. G., Krinner, G., Marotzke, J.,
 492 ... Zickfeld, K. (2021). Technical summary [Book Section]. In V. Masson-
 493 Delmotte et al. (Eds.), *Climate change 2021: The physical science basis. con-*
 494 *tribution of working group i to the sixth assessment report of the intergovern-*
 495 *mental panel on climate change* (chap. 1). Cambridge, United Kingdom and
 496 New York, NY, USA: Cambridge University Press. Retrieved from [https://](https://www.ipcc.ch/report/ar6/wg1/downloads/report/IPCC_AR6_WGI_TS.pdf)
 497 www.ipcc.ch/report/ar6/wg1/downloads/report/IPCC_AR6_WGI_TS.pdf
- 498 Boers, N. (2021). Observation-based early-warning signals for a collapse of the
 499 Atlantic Meridional Overturning Circulation. *Nature Climate Change*, 11(8),
 500 680–688. Retrieved from <http://dx.doi.org/10.1038/s41558-021-01097-4>
 501 doi: 10.1038/s41558-021-01097-4
- 502 Boulton, C. A., Lenton, T. M., & Boers, N. (2022). Pronounced loss of Amazon
 503 rainforest resilience since the early 2000s. *Nature Climate Change*, 12(March).
 504 doi: 10.1038/s41558-022-01287-8
- 505 Caesar, L., McCarthy, G. D., Thornalley, D. J., Cahill, N., & Rahmstorf, S. (2021).
 506 Current Atlantic Meridional Overturning Circulation weakest in last millen-
 507 nium. *Nature Geoscience*, 14(3), 118–120. Retrieved from [http://dx.doi](http://dx.doi.org/10.1038/s41561-021-00699-z)
 508 [.org/10.1038/s41561-021-00699-z](http://dx.doi.org/10.1038/s41561-021-00699-z) doi: 10.1038/s41561-021-00699-z
- 509 Carvalho, N. S., Anderson, L. O., Nunes, C. A., Pessôa, A. C., Silva Junior, C. H.,
 510 Reis, J. B., ... Aragão, L. E. (2021). Spatio-Temporal variation in dry season
 511 determines the Amazonian fire calendar. *Environmental Research Letters*,
 512 16(12). doi: 10.1088/1748-9326/ac3aa3
- 513 Chang, P., Zhang, R., Hazeleger, W., Wen, C., Wan, X., Ji, L., ... Seidel, H. (2008).
 514 Oceanic link between abrupt changes in the north Atlantic ocean and the
 515 African monsoon. *Nature Geoscience*, 1(7), 444–448. doi: 10.1038/ngeo218
- 516 Drijfhout, S. S., Weber, S. L., & van der Swaluw, E. (2011). The stabil-
 517 ity of the MOC as diagnosed from model projections for pre-industrial,
 518 present and future climates. *Climate Dynamics*, 37(7-8), 1575–1586. doi:
 519 10.1007/s00382-010-0930-z
- 520 Frajka-Williams, E., Moat, B., Smeed, D., Rayner, D., Johns, W., Baringer, M., ...

- 521 Collins, J. (2021). *Atlantic meridional overturning circulation observed by*
 522 *the rapid-mocha-wbts (rapid-meridional overturning circulation and heatflux*
 523 *array-western boundary time series) array at 26n from 2004 to 2020 (v2020.1).*
 524 doi: 10.5285/cc1e34b3-3385-662b-e053-6c86abc03444
- 525 Good, P., Boers, N., Boulton, C. A., Lowe, J. A., & Richter, I. (2021). How might a
 526 collapse in the Atlantic Meridional Overturning Circulation affect rainfall over
 527 tropical South America? *Climate Resilience and Sustainability*(November),
 528 1–13. doi: 10.1002/cli2.26
- 529 Häggi, C., Chiessi, C. M., Merkel, U., Mulitza, S., Prange, M., Schulz, M., & Sche-
 530 fuß, E. (2017). Response of the Amazon rainforest to late Pleistocene cli-
 531 mate variability. *Earth and Planetary Science Letters*, *479*, 50–59. Re-
 532 trieved from <http://dx.doi.org/10.1016/j.epsl.2017.09.013> doi:
 533 10.1016/j.epsl.2017.09.013
- 534 Henry, L. G., McManus, J. F., Curry, W. B., Roberts, N. L., Piotrowski, A. M.,
 535 & Keigwin, L. D. (2016). North Atlantic ocean circulation and abrupt cli-
 536 mate change during the last glaciation. *Science*, *353*(6298), 470–474. doi:
 537 10.1126/science.aaf5529
- 538 Jackson, L. C., Asenjo, E. A. D., Bellomo, K., Danabasoglu, G., Haak, H., Hu, A.,
 539 ... Swingedouw, D. (2022). Understanding AMOC stability : the North At-
 540 lantic Hosing Model Intercomparison Project. *Geoscientific Model Development*
 541 *Discussions*(November), 1–32. Retrieved from [https://gmd.copernicus.org/](https://gmd.copernicus.org/preprints/gmd-2022-277/)
 542 [preprints/gmd-2022-277/](https://gmd-2022-277/) doi: 10.5194/gmd-2022-277
- 543 Jackson, L. C., Kahana, R., Graham, T., Ringer, M. A., Woollings, T., Mecking,
 544 J. V., & Wood, R. A. (2015). Global and European climate impacts of a slow-
 545 down of the AMOC in a high resolution GCM. *Climate Dynamics*, *45*(11-12),
 546 3299–3316. Retrieved from <http://dx.doi.org/10.1007/s00382-015-2540-2>
 547 doi: 10.1007/s00382-015-2540-2
- 548 Jackson, L. C., & Wood, R. A. (2018). Hysteresis and Resilience of the AMOC in an
 549 Eddy-Permitting GCM. *Geophysical Research Letters*, *45*(16), 8547–8556. doi:
 550 10.1029/2018GL078104
- 551 Lee, J. Y., Marotzke, J., Bala, G., Cao, L., Corti, S., Dunne, J. P., ... Zhou, T.
 552 (2021). Future global climate: Scenario-based projections and near-term infor-
 553 mation [Book Section]. In V. Masson-Delmotte et al. (Eds.), *Climate change*
 554 *2021: The physical science basis. contribution of working group i to the sixth*
 555 *assessment report of the intergovernmental panel on climate change* (chap. 4).
 556 Cambridge, United Kingdom and New York, NY, USA: Cambridge University
 557 Press. Retrieved from [https://www.ipcc.ch/report/ar6/wg1/downloads/](https://www.ipcc.ch/report/ar6/wg1/downloads/report/IPCC_AR6_WGI_Chapter_04.pdf)
 558 [report/IPCC_AR6_WGI_Chapter_04.pdf](https://www.ipcc.ch/report/ar6/wg1/downloads/report/IPCC_AR6_WGI_Chapter_04.pdf)
- 559 Liu, W., Xie, S. P., Liu, Z., & Zhu, J. (2017). Overlooked possibility of a collapsed
 560 atlantic meridional overturning circulation in warming climate. *Science Ad-*
 561 *vances*, *3*(1), 1–8. doi: 10.1126/sciadv.1601666
- 562 Liu, Y., Chiang, J. C., Chou, C., & Patricola, C. M. (2014). Atmospheric
 563 teleconnection mechanisms of extratropical North Atlantic SST influ-
 564 ence on Sahel rainfall. *Climate Dynamics*, *43*(9-10), 2797–2811. doi:
 565 10.1007/s00382-014-2094-8
- 566 Marzin, C., Kallel, N., Kageyama, M., Duplessy, J. C., & Braconnot, P. (2013).
 567 Glacial fluctuations of the Indian monsoon and their relationship with North
 568 Atlantic climate: New data and modelling experiments. *Climate of the Past*,
 569 *9*(5), 2135–2151. doi: 10.5194/cp-9-2135-2013
- 570 Moon, S., & Ha, K. J. (2020). Future changes in monsoon duration and precip-
 571 itation using CMIP6. *npj Climate and Atmospheric Science*, *3*(1), 1–7.
 572 Retrieved from <http://dx.doi.org/10.1038/s41612-020-00151-w> doi:
 573 10.1038/s41612-020-00151-w
- 574 Mosblech, N. A., Bush, M. B., Gosling, W. D., Hodell, D., Thomas, L., Van Cal-
 575 steren, P., ... Van Woesik, R. (2012). North Atlantic forcing of Amazonian

- 576 precipitation during the last ice age. *Nature Geoscience*, 5(11), 817–820. doi:
577 10.1038/ngeo1588
- 578 Orihuela-Pinto, B., England, M. H., & Taschetto, A. S. (2022). Interbasin and inter-
579 hemispheric impacts of a collapsed Atlantic Overturning Circulation. *Nature*
580 *Climate Change*. doi: 10.1038/s41558-022-01380-y
- 581 Parsons, L. A., Yin, J., Overpeck, J. T., Stouffer, R. J., & Malyshev, S. (2014).
582 Influence of the atlantic meridional overturning circulation on the monsoon
583 rainfall and carbon balance of the American tropics. *Geophysical Research*
584 *Letters*, 41(1), 146–151. doi: 10.1002/2013GL058454
- 585 Rahmstorf, S. (2002). NAT(419,207)-circulation. , 419(September), 207–214.
- 586 Rahmstorf, S., Crucifix, M., Ganopolski, A., Goosse, H., Kamenkovich, I., Knutti,
587 R., . . . Weaver, A. J. (2005). Thermohaline circulation hysteresis: A
588 model intercomparison. *Geophysical Research Letters*, 32(23), 1–5. doi:
589 10.1029/2005GL023655
- 590 Romanou, A., Rind, D., Jonas, J., Miller, R., Kelley, M., Russell, G., . . . Schmidt,
591 G. A. (2023). Stochastic Bifurcation of the North Atlantic Circulation Under
592 a Mid-Range Future Climate Scenario With The NASA-GISS ModelE.
593 *Journal of Climate*, 1 - 49. Retrieved from [https://journals.ametsoc.org/
594 view/journals/clim/aop/JCLI-D-22-0536.1/JCLI-D-22-0536.1.xml](https://journals.ametsoc.org/view/journals/clim/aop/JCLI-D-22-0536.1/JCLI-D-22-0536.1.xml) doi:
595 10.1175/JCLI-D-22-0536
- 596 Sandeep, N., Swapna, P., Krishnan, R., Farneti, R., Prajeesh, A. G., Ayantika,
597 D. C., & Manmeet, S. (2020). South Asian monsoon response to weakening
598 of Atlantic meridional overturning circulation in a warming climate. *Climate*
599 *Dynamics*, 54(7-8), 3507–3524. Retrieved from [https://doi.org/10.1007/
600 s00382-020-05180-y](https://doi.org/10.1007/s00382-020-05180-y) doi: 10.1007/s00382-020-05180-y
- 601 Schneider, U., Becker, A., Finger, P., Rustemeier, E., & Ziese, M. (2020). *Gpcc*
602 *full data monthly product version 2020 at 0.25°: Monthly land-surface pre-*
603 *cipitation from rain-gauges built on gts-based and historical data.* doi:
604 10.5676/DWD_GPCC/FD_M_V2020_025
- 605 Stommel, H. (1961). Thermohaline Convection with Two Stable Regimes of Flow.
606 *Tellus*, 13(2), 224–230. doi: 10.3402/tellusa.v13i2.9491
- 607 Stouffer, R. J., Yin, J., Gregory, J. M., Dixon, K. W., Spelman, M. J., Hurlin, W.,
608 . . . Weber, S. L. (2006). Investigating the causes of the response of the
609 thermohaline circulation to past and future climate changes. *Journal of Cli-*
610 *mate*, 19(8), 1365 - 1387. Retrieved from [https://journals.ametsoc.org/
611 view/journals/clim/19/8/jcli3689.1.xml](https://journals.ametsoc.org/view/journals/clim/19/8/jcli3689.1.xml) doi: [https://doi.org/10.1175/
612 JCLI3689.1](https://doi.org/10.1175/JCLI3689.1)
- 613 Sun, Y., Clemens, S. C., Morrill, C., Lin, X., Wang, X., & An, Z. (2012). Influ-
614 ence of Atlantic meridional overturning circulation on the East Asian winter
615 monsoon. *Nature Geoscience*, 5(1), 46–49. doi: 10.1038/ngeo1326
- 616 Wang, B., Biasutti, M., Byrne, M. P., Castro, C., Chang, C. P., Cook, K., . . . Zhou,
617 T. (2021). Monsoons climate change assessment. *Bulletin of the American*
618 *Meteorological Society*, 102(1), E1-E19. doi: 10.1175/BAMS-D-19-0335.1
- 619 Wassenburg, J. A., Vonhof, H. B., Cheng, H., Martínez-García, A., Ebner, P. R., Li,
620 X., . . . Haug, G. H. (2021). Penultimate deglaciation Asian monsoon response
621 to North Atlantic circulation collapse. *Nature Geoscience*, 14(12), 937–941.
622 doi: 10.1038/s41561-021-00851-9
- 623 WRCP, W. C. R. P. (n.d.). *The global monsoon systems.* Retrieved from [https://
624 www.wcrp-climate.org/documents/monsoon_factsheet.pdf](https://www.wcrp-climate.org/documents/monsoon_factsheet.pdf)
- 625 Yu, L., Gao, Y. Q., Wang, H. J., Guo, D., & Li, S. L. (2009). The responses of East
626 Asian Summer monsoon to the North Atlantic Meridional Overturning Circu-
627 lation in an enhanced freshwater input simulation. *Chinese Science Bulletin*,
628 54(24), 4724–4732. doi: 10.1007/s11434-009-0720-3